EurJIC
European Journal of Inorganic Chemistry

Research Article
doi.org/10.1002/ejic.202300433

Chemistry Europe
European Chemical Societies Publishing

www.eurjic.org

Special Collection

Single-Source Precursors for the Chemical Vapor Deposition of Iron Germanides

Thomas Büttner,[a] Oliver Janka,[b] Volker Huch,[c] Debabrata Dhara,[d] Anukul Jana,[d] and David Scheschkewitz*[a]

Binary iron-germanium phases are promising materials in magnetoelectric, spintronic or data storage applications due to their unique magnetic properties. Previous protocols for preparation of Fe_xGe_y thin films and nanostructures typically involve harsh conditions and are challenging in terms of phase composition and homogeneity. Herein, we report the first example of single source chemical vapor deposition (CVD) of Fe_xGe_y films. The appreciable volatility of $[Ge[Fe_2(CO)_8]_2]$, $[Cl_2GeFe(CO)_4]_2$ and $^{Me_2iPr_2}NHC\cdot GeCl_2\cdot Fe(CO)_4$ allowed for their application as precursors under standard CVD conditions ($^{Me_2iPr_2}NHC$ = 1,3-diisopropoyl-4,5-dimethylimidazol-2-ylidene). The thermal decomposition products of the precursors were characterized by TGA and powder XRD. Deposition experiments in a cold-wall CVD reactor resulted in dense films of Fe_xGe_y. During the optimization of synthetic conditions for precursor preparation the new iron-germanium cluster $Cl_2Ge[Fe_2(CO)_8]Ge[Fe_2(CO)_8]$ was obtained in experiments with a higher stoichiometric ratio of $GeCl_2\cdot$1,4-dioxane vs. $Fe_2(CO)_9$.

Introduction

Intermetallic phases of iron and germanium have been subject of research for more than 50 years.[1] Besides the intriguing complexity of the Fe–Ge binary system, these phases exhibit a variety of magnetic properties,[2] which make them promising materials for magnetoelectronic, magnetocaloric and magnetic memory applications.[3] The helimagnetic FeGe is of particular interest; the formation of magnetic skyrmion crystals near room temperature has been proven for thin films of this material prepared by argon ion thinning of a mechanically polished sample.[4]

In view of the rising interest in iron germanides, new protocols for their preparations especially in the form of thin films are needed. Usually, these materials are prepared by smelting of the elements or in solid state reactions in the desired stoichiometry.[5] Thin films are accessible by application of ion beams[4] or sputtering of iron on germanium wafers at high temperatures.[6] These relatively harsh reaction conditions restrict the field of possible applications. Methods based on molecular precursors could provide access to the deposition of iron germanides in nanostructured thin films from the gas or solution phase with facile control of composition, thickness, morphology and hence tunable magnetic and other properties. Only a few methods for the deposition of iron germanides from molecular precursors are known. Schaak *et al.* synthesized FeGe and Fe_3Ge_2 nanostructures starting from GeI_4 and $Fe(CO)_5$ in oleyl amine at 260 °C or 300 °C respectively.[7] Delpech *et al.* obtained Fe_5Ge_3 nanoparticles by thermal decomposition of germylene/ironcarbonyl complexes in mesitylene.[8] [BMIm][$(GeI_3)_2Fe(CO)_3I$] (BMIm = 1-butyl-3-methylimidazolium) has served as an single source precursor (SSP) for bimetallic Ge–Fe nanoparticles in ionic liquids.[9] A chemical vapor transport reaction of elemental Ge and FeI_2 resulted in nanowires of ferromagnetic Fe_4Ge_3 or FeGe depending on the experimental conditions.[10]

In contrast to the corresponding processes for the preparation of transition metal silicides such as FeSi, CoSi and MnSi,[11] the single source chemical vapor deposition (CVD) of transition metal germanides is completely unexplored despite numerous iron- and germanium-containing molecular species (Scheme 1),[12] which are not only sufficiently small and should hence provide a suitable evaporation rate but also contain ligands that should easily cleave at elevated temperatures. Early examples of such candidates are the bis(trihalogermyl)irontetracabonyls **I** and dihalogermylene-iron

[a] *T. Büttner, Prof. Dr. D. Scheschkewitz*
Krupp-Chair for General and Inorganic Chemistry
Saarland University
66123 Saarbrücken (Germany)
E-mail: scheschkewitz@mx.uni-saarland.de

[b] *Dr. O. Janka*
Inorganic Solid State Chemistry
Saarland University
66123 Saarbrücken (Germany)

[c] *Dr. V. Huch*
Service Center X-ray Diffraction
Saarland University
66123 Saarbrücken (Germany)

[d] *D. Dhara, Prof. Dr. A. Jana*
Tata Institute of Fundamental Research
Centre for Interdisciplinary Sciences
Hyderabad 500075 (India)

Supporting information for this article is available on the WWW under https://doi.org/10.1002/ejic.202300433

Special Collection *Part of the Wöhler Vereinigung für Anorganische Chemie Prize Winners Special Collection.*

Research Article
doi.org/10.1002/ejic.202300433

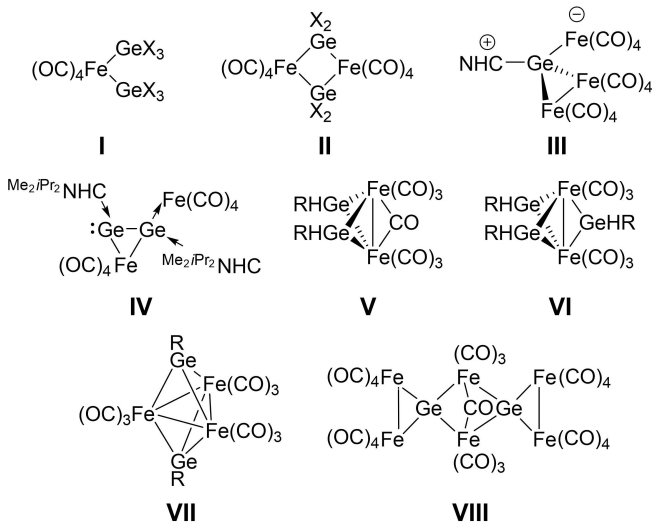

Scheme 1. Some reported Ge–Fe carbonyl compounds (X=Cl, Br, I; ^{Me_2iPr_2}NHC = 1,3-diisopropoyl-4,5-dimethylimidazol-2-ylidene; R=Me, Et).

carbonyl complexes reported as dimers of the form $[X_2Ge{\cdot}Fe(CO)_4]_2$ **II** (X=Cl, Br, I). In both cases, the preparation involves long reaction times of several days and mediocre yields.[13] In presence of donors, an equilibrium of **II** with the monomeric, donor-stabilized $L{\cdot}GeX_2{\cdot}Fe(CO)_4$ was reported (L = donating neutral ligand).[14] Jutzi and Steiner described the sole formation of the solvent-stabilized germylene complex $thf{\cdot}GeCl_2{\cdot}Fe(CO)_4$ **1** upon reaction of $GeCl_2$/1,4-dioxane complex with $Fe_2(CO)_9$ in thf (Scheme 1).[15] The analogous reaction of ^{Me_2iPr_2}NHC·$GeCl_2$ results in the corresponding ^{Me_2iPr_2}NHC·$GeCl_2{\cdot}Fe(CO)_4$[16] (**3**), which can be further derivatized by substitution of the chlorides using methyl lithium[17] and by reduction either to an NHC-substituted $[GeFe_3]$ cluster **III** through further treatment with $Fe_2(CO)_9$[18] or to the dimer $[^{Me_2iPr_2}NHC{\cdot}Ge{\cdot}Fe(CO)_4]_2$ **IV** using potassium/graphite.[16b] Larger iron-germanium clusters are accessible by the reaction of organylgermanes with ironcarbonyls as part of typically complex reaction mixtures from which propellane-stuctured **V** and **VI**,[19,20] the trigonal-bipyramidal **VII**[19] and the *spiro*-clusters **VIII**[21] and **4**[19,21] were isolated.

Herein, we report improved synthetic procedures for selected small Ge–Fe carbonyl compounds. More importantly, these compounds were successfully employed as single-source precursors (SSP) in the first chemical vapor deposition of Fe_xGe_y thin films.

Results and Discussion

Precursor Preparation and Characterization

We anticipated that the presence of NHCs in the precursor would both lead to reduced volatility and a higher risk of carbon or nitrogen incorporation into the deposited films. We therefore chose the thf complex **1** as prime candidate as SSP for CVD of iron germanides. Following the procedure reported by Jutzi and Steiner,[15] treatment of $GeCl_2$/1,4-dioxane with one equivalent of $Fe_2(CO)_9$ at −80 °C in thf resulted in the precipitation of a yellow to orange powder after addition of an equal volume of hexane (or upon extended storage at −80 °C). IR spectra of the substance, however, clearly indicated the formation of dimer **2** instead of **1** with bands identical to those reported by Kummer and Graham (Scheme 2).[13] The monomeric thf adduct **1**, previously reported as the sole product of this reaction,[15] remained undetected in the isolated solid product in our hands. Dimer **2** can be further purified by sublimation at 80 °C and 10^{-2} mbar and thus exhibits a suitable volatility for CVD experiments despite its higher molecular weight compared to **1**. In line with the octahedral coordination of Fe, the $^{13}C\{^1H\}$ NMR spectrum of **2** in C_6D_6 exhibits two resonances (δ = 204.0 and 197.0 ppm) in a 1:1 ratio, representing the axial and equatorial CO ligands. Addition of thf or changing the solvent to thf-d_8 does not affect the NMR spectra at all, which implies that the dimeric form **2** is still present under these conditions as the terminal $Fe(CO)_4$ in **1** would only give rise to a single resonance due to rapid Berry pseudorotation.

The structure of **2** was confirmed for the first time by single crystal X-ray diffraction analysis on single crystals obtained from a hot saturated solution in hexane (Figure 1). It crystallizes in the tetragonal space group $I4_1/acd$ with only a quarter of the molecule in the asymmetric unit. In the solid state, the molecular unit of **2** exhibits the same configuration as other known binuclear complexes of the type $[Fe_2(\mu\text{-}GeR_2)_2(CO)_8]$.[22] As both Fe1 and Ge1 reside on special positions in the horizontal mirror plane, the $[Fe_2Ge_2]$ ring is planar by definition. While the coordination geometry of Ge1 is nearly ideally

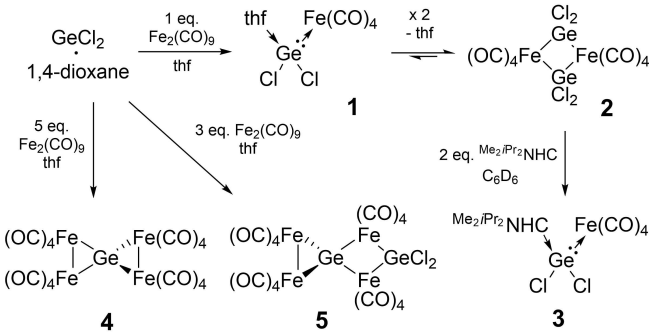

Scheme 2. Preparation of precursor molecules **2**–**4** (^{Me_2iPr_2}NHC = 1,3-diisopropoyl-4,5-dimethylimidazol-2-ylidene).

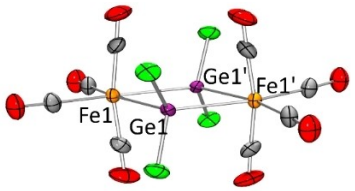

Figure 1. Molecular structure of **2** (thermal ellipsoids at 50% probability). Selected bond lengths [Å] and angles [°]: Ge1-Fe1 2.4084(3), Ge1-Ge1′ 2.8960(4), Fe1-Fe1′ 3.8487(4), Ge1-Cl1 2.1842(4), Fe1-Ge1-Fe1′ 106.08(1), Ge1-Fe1-Ge1′ 73.92(1).

Research Article
doi.org/10.1002/ejic.202300433

tetrahedral, the octahedral environment at Fe1 is significantly distorted. The axial CO ligands are inclined to the center of the molecule (C_{ax}-Fe1-Fe1′: 85.00(5)°). The Ge1-Fe1-Ge1′ angle is more acute (73.92(1)°) and the angle between the equatorial CO ligands consequently widened (C_{eq}-Fe-C_{eq}: 100.99(9)°). According to Alvarez *et al.*, the presence of chlorine substituents in $[M_2E_2]$ rings (in which M is a transition metal and E is a group 14 element) causes a noticeable ring contraction.[22] Fully in line with this, the fourfold chlorinated compound **2** has the shortest iron-germanium bond length (Fe1-Ge1 2.4084(3) Å) so far reported for $[Fe_2(\mu\text{-}GeR_2)_2(CO)_8]$ compounds. While Fe—Fe distance of 3.8487(4) Å is still in the typical range, the Ge1-Ge1′ distance of 2.8960(4) Å is significantly shortened although a through-space bonding interaction of the two germylene fragments is considered to be unlikely.[22]

If an equilibrium existed between **1** and **2**, it should allow for the synthesis of other base-stabilized dichlorogermylene/iron carbonyl complexes. Indeed, the addition of a solution of two equivalents of ^{Me_2iPr_2}NHC to a suspension of **2** (both in C_6D_6) results in dissolution of the solid and a color change from yellow to brown-orange. $^{13}C\{^1H\}$ and ^1H NMR (Figure S4 and S5) reveal the essentially quantitative formation of $^{Me_2iPr_2}NHC\cdot GeCl_2\cdot Fe(CO)_4$ **3**, which had previously been prepared by the reversed reaction sequence, i.e. initial reaction of $GeCl_2\cdot$1,4-dioxane with the NHC prior to complexation to the $Fe(CO)_4$ fragment.[16]

As we reported before, an excess of $Fe_2(CO)_9$ can reduce $^{Me_2iPr_2}NHC\cdot GeCl_2\cdot Fe(CO)_4$ to $^{Me_2iPr_2}NHC\cdot Ge[Fe(CO)_4]_3$.[18] Accordingly, the reaction of a fivefold excess of $Fe_2(CO)_9$ with $GeCl_2\cdot$1,4-dioxane in thf for three days results in complete reduction of the germanium center yielding the *spiro*-compound **4** as a red powder in 58% yield. Single crystals were obtained from hot saturated hexane solution and an X-ray diffraction study confirmed the structure reported by Melzer and Weiss.[23] Compound **4** frequently occurs as side product in germanium ironcarbonyl chemistry[19–21,24] and can be alternatively prepared from GeH_4 with $Fe_2(CO)_9$ in slightly lower yields.[25] A single resonance is observed in $^{13}C\{^1H\}$ NMR in C_6D_6 at $\delta = 208.6$ ppm. Compound **4** is suitably volatile for use as CVD precursor; it can be sublimed at 80 °C and 10^{-2} mbar without decomposition. Although it is reported to be air-stable,[23] we found that it darkens in color after several days of exposure to air and forms insoluble, undefined decomposition products. Storage under argon and below 0 °C is therefore recommended.

When the reaction is carried out with three equivalents of Fe_2CO_9, a mixture of products results that can be separated by flash chromatography (silica, hexane). As **4** and **5** appear to gradually decompose on silica, the separation should be performed as quickly as possible. In order of elution the following products are obtained: $Fe_3(CO)_{12}$ as a green fraction, **4** (red-orange fraction, 12% yield) and a hitherto unreported side-product **5**. The collected dark-red hexane fraction of **5** was concentrated and stored at −20 °C to result in red crystals (7% yield in respect to germanium) suitable for X-ray diffraction (Figure 2).

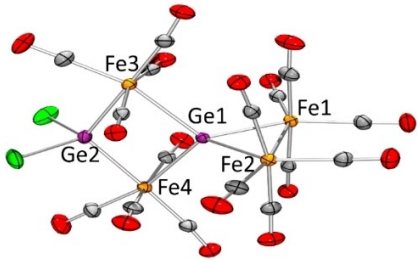

Figure 2. Molecular structure of **5** (thermal ellipsoids at 50% probability). Selected bond lengths [Å] and angles [°]: Fe1-Fe2 2.7932(3), Ge1-Fe1 2.4288(2), Ge1-Fe2 2.4138(2), Ge1-Fe3 2.5873(2), Ge1-Fe4 2.5873(2), Ge2-Fe3 2.3780(2), Ge2-Fe4 2.3732(2), Fe1-Ge1-Fe2 70.450(7), Fe3-Ge1-Fe4 97.167(7), Fe3-Ge2-Fe4 109.579(8), Ge1-Fe3-Ge2 76.569(7), Ge1-Fe4-Ge2 76.613(7).

The crystal structure of **5** can be regarded as a hybrid of the planar $[Fe_2Ge_2]$ ring in **2** and the *spiro*-cluster **4**. As in **4**,[23] Ge1 in **5** has a distorted tetrahedral coordination, with the terminal $Ge[Fe_2(CO)_8]$ fragment featuring a similar Fe1-Ge1-Fe2 angle (70.450(7)°) and iron-germanium distances (Fe1-Ge1 2.4288(2), Fe2-Ge1 2.4138(2) Å) as the corresponding values in **4** (71° and 2.41 Å). The Fe3-Ge1-Fe4 angle of 97.167(7)° falls between the values of the corresponding angles in **4** and **2** (71°[16b] and 106.08(1)°), which results in a deformation of the $[Fe_2Ge_2]$ ring. The Fe3-Ge2-Fe4 angle at the $GeCl_2$ fragment is also slightly widened to 109.579(8)°. While the Ge—Fe bonds to the $GeCl_2$ fragment (Fe3-Ge2 2.3780(2), Fe4-Ge2 2.3732(2) Å) are even shorter than in **2** (2.4084(3) Å), the adjacent bonds to Ge1 (Fe3-Ge1 2.5873(2), Fe4-Ge1 2.5892(2) Å) are considerably longer than in **2** and **4**. This indicates a somewhat weaker interaction of the $Cl_2Ge(Fe(CO)_4)_2$ and $GeFe_2(CO)_8$ fragments compared to that in the symmetrical dimer **2**. The coordination octahedra of all iron centers are distorted with the axial CO ligands of Fe3 and Fe4 and all CO ligands of Fe1 and Fe2 bending towards the center of the molecule.

The nature of **5** as a hybrid molecule of **2** and **4** is also reflected in its $^{13}C\{^1H\}$ NMR spectrum, which features three signals in a ratio of 2:1:1. They represent the equivalent CO ligands of the terminal $Ge[Fe_2(CO)_8]$ fragment at $\delta = 207.1$ ppm and the axial and equatorial CO ligands at $\delta = 200.8$ and 198.6 ppm with similar chemical shifts as those of **2** and **4**. Since **5** is at present only available in low yields, its use as a CVD precursor was not further pursued. An attempt to deliberately synthesize **5** by combination of **4** and one equivalent of $GeCl_2\cdot$1,4-dioxane did not result in any conversion.

Decomposition Behaviour

Compounds **2**, **3** and **4** were chosen as precursors for thermal decomposition based on their moderate molecular weight (and thus presumably sufficient volatility) and the presence of *a priori* thermally cleavable ligands at Fe and Ge. Transition metal carbonyl complexes are well-known precursor molecules for preparation of high purity metal films and materials.[26] NHC complexes have been employed as deposition precursors as

Research Article
doi.org/10.1002/ejic.202300433

well; for instance, complexes with small alkyl-substituted NHCs of the type $[Co(CO)(NO)(NHC)_2]$ and $[Co(CO)_2(NO)(NHC)]$ served as low temperature precursors in the CVD of thin cobalt films.[27] In addition, Rivard *et al.* reported that the decomposition of $^{Me_2}NHC \cdot GeH_2 \cdot BH_3$ in toluene at 100 °C leads to the formation of thin germanium layers.[28] Metal halides can be thermally decomposed to form metal films as well, although usually only at high temperatures. Therefore, they are typically used in combination with hydrogen as a reducing carrier gas.[29]

Indeed, the thermogravimetric analyses (TGA) of the of chloride-containing **2** and **3** show relatively higher onset temperatures for decomposition compared to chloride-free **4** (Table 1). For **2**, TGA reveals a complex decomposition pathway that consists of four steps (Figure S11) and ends with a residual mass of 26.3% at 650 °C. As the mass of the residue is significantly lower than expected for FeGe (41.3%), the loss of heavier molecular fragments beyond the mere elimination of the ligands must occur. Decomposition studies on compounds of type $(thf)GeCl_2M(CO)_5$ (M=Cr, W) reportedly resulted in the formation of germanium-poor phases as well, which had been ascribed to the formation of volatile $GeCl_4$.[30] Monitoring of the pyrolysis exhaust by IR-spectroscopy confirms that the first decomposition step at $T_{onset} = 210$ °C only involves carbon monoxide evolution, which is in line with the observed mass loss of 35.6% (theoretical mass loss of 36.0% for departure of all CO ligands) and indicating a net composition of "$FeGeCl_2$" after this step. The following three decomposition steps are dominated by the evolution of HCl. The counterintuitive formation of HCl might be due to the hydrolysis of intermittently formed germanium chlorides by moisture in the carrier gas, which would also explain our inability to detect any volatile germanium species at the IR detector. In combination with the absence of the comparatively stable $Fe(CO)_5$ in the pyrolysis exhaust, we nonetheless assume the loss of germanium and accordingly the formation of a germanium-poor phase such as Fe_5Ge_3, which is also in good agreement with the final residual mass value (26.6% theoretical mass for Fe_5Ge_3 formation vs. 26.3% observed residual mass). In contrast, compound **4** exhibits a single mass loss at $T_{onset} = 220$ °C to 41.1% corresponding closely to the theoretical value resulting from the departure of all CO ligands (39.8%) and thus an Fe_4Ge residue.

Table 1. Thermogravimetric characteristics of compounds **2**–**4**.

	$T_{dec.}$ [°C]	Residual mass [%]		Assumed phase
		observed	theoretical[a]	
2	650	26.3	26.6	Fe_5Ge_3
3	550	25.6	26.1	FeGe
4	220	40.1	39.8	Fe_4Ge

[a] Value for the assumed phases.

Thin Film Preparation

The designated precursors **2**, **3** and **4** were tested in a typical horizontal cold-wall CVD-reactor.[31] The deposition was carried out on silicon or glass substrates with an internal pressure range of 10^{-3} to 10^{-2} mbar, depending on the precursor choice. To enhance the precursor volatility, the precursor reservoir and reactor chamber were subjected to additional heating (for details see Supporting Information).

The obtained films were characterized by tapping mode atomic force microscopy (AFM) and scanning electron microscopy (SEM) for topography as well as energy dispersive spectroscopy (EDX) and X-ray diffraction (XRD) for composition and phase analysis. The film thickness was estimated by AFM imaging of a deliberately scratched sample.

Precursor **2** was evaporated at 80 °C and $2 \cdot 10^{-2}$ mbar and deposited at 650 °C for 2.5 h. Even after this relatively short time, the substrate is densely covered with irregular shaped grains with diameters of 100 nm up to 400 nm according to atomic force micrographs (Figure 3). Elemental analysis of the film by EDX reveals an Fe:Ge ratio of 62:38, which is in reasonable agreement with the theoretical value for the Fe_5Ge_3 phase (62.5:37.5). The detection of carbon with a relative amount of 10 at% according to EDX indicates a certain degree of CO disproportionation. In contrast, there is no evidence for chlorine incorporation. Powder XRD of samples prepared on glass were featureless, either due to low film thickness or the amorphous nature of the deposited film. Even an extension of the deposition time to 18 h does not increase crystallinity significantly (Figure S19) so that the phase could not be determined by powder XRD. The film thickness was estimated to approximately 150 nm (Figure S15), which suggests that the poor XRD data is rather due to the amorphous nature of the deposited material than to a low film thickness. Furthermore, **2** was pyrolyzed in bulk at 650 °C for 7 days to clarify the nature of its decomposition product. While the powder diffraction pattern of the thus obtained material exhibits indeed some crystallinity, the multitude of reflections could not be indexed suggesting a complicated mixture (Figure S20).

Compound **3** showed a significantly lower evaporation tendency than **2**. After 6 h of deposition with **3**, the substrate is covered with densely packed particles as seen in the AFM and SEM images (Figure 4). Their dimensions were identified by atomic force micrographs as 58 nm in diameter and 11 nm in height on average. With a smaller scan size (Figure 4D and 4E), similar features of lower prominence are observed. In general, more densely populated domains are visible next to areas of lower particle density, even though the particle size does not differ significantly. By bearing analysis of the AFM dataset, an overall coverage of the surface of 79% was determined. The Fe–Ge ratio is 60:40 according to EDX, which is a slightly higher iron content than expected but consistent with the thermogravimetric analysis. As in the case of **2**, no chlorine was detected in the film. Unfortunately, the obtained films were equally unsuitable for powder XRD due to the low film thickness or its amorphous nature. A Si-K_α signal of significant intensity supports the former interpretation.

Research Article
doi.org/10.1002/ejic.202300433

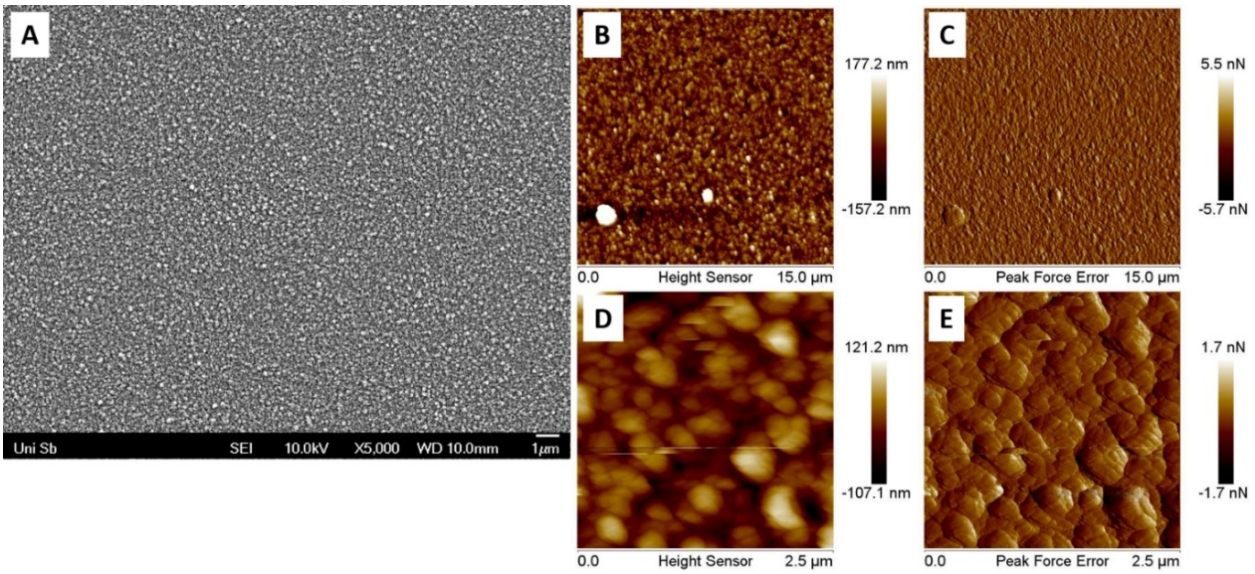

Figure 3. Scanning electron micrograph (**A**) and scanning probe micrographs (**B**–**E**) of iron germanide film by CVD of **2** at 650 °C.

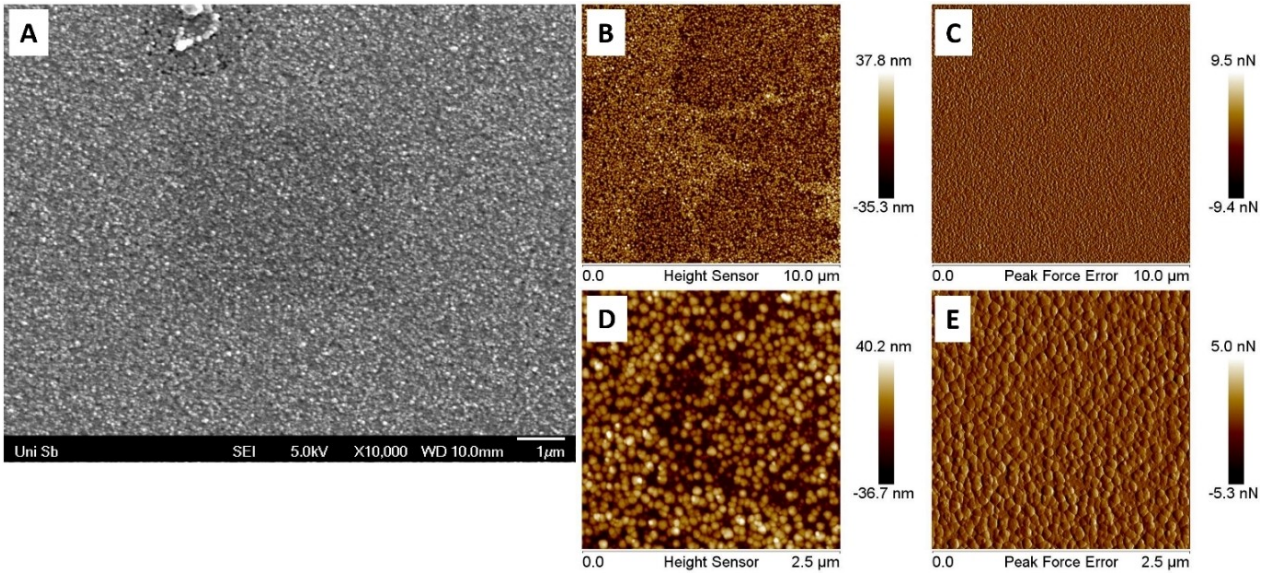

Figure 4. Scanning electron micrograph (**A**) and scanning probe micrographs (**B**–**E**) of particle deposits by CVD of **3** at 525 °C.

In order to still obtain an idea of possible crystallographic phases, compound **3** was pyrolyzed in bulk at 550 °C under a protecting atmosphere of argon. The resulting gray powder was investigated by powder X-ray diffraction using an air-sensitivity sample holder (Figure 5). As no differences of the diffraction pattern were observed during a repeat run under air, stability towards nitrogen, oxygen and moisture can be assumed. Comparison with the Pearson database[32] indicated the formation of hexagonal $Fe_{2-x}Ge$ ($x = 0$–0.7) crystallizing in the $Co_{1.75}Ge$ type structure ($P6_3/mmc$) as main component along with minor amounts of FeGe observed both in the cubic FeSi ($P2_13$) and the hexagonal CoSn ($P6/mmm$) type structures. Rietveld refinement led to a composition of $Fe_{1.66(1)}Ge$ ($x = 0.44$) along with lattice parameters of $a = 397.85(2)$ and $c = 499.87(3)$ pm for the main phase (93.5(3) at%). FeGe in the FeSi type exhibits a lattice parameter of $a = 470.61(4)$ pm with a phase contribution of 1.0(3) at% while FeGe in the CoSn type has lattice parameters of $a = 503.24(6)$ and $c = 416.55(5)$ pm and a 5.5(3) at% phase contribution. Note that these small phase contributions and the relatively low signal-to-noise ratio leaves considerable room for alternative interpretations.

In comparison to the other tested substances, precursor **4** shows a high volatility and permits a low decomposition temperature of 220 °C. After 5 h of deposition and a target temperature of 360 °C,[33] the substrates are visibly coated with films of silvery metallic appearance. SEM and AFM images (Figure 6 A–C) reveal dense films, formed by round grains with a diameter of 100 nm. With raising target temperatures, the

Research Article
doi.org/10.1002/ejic.202300433

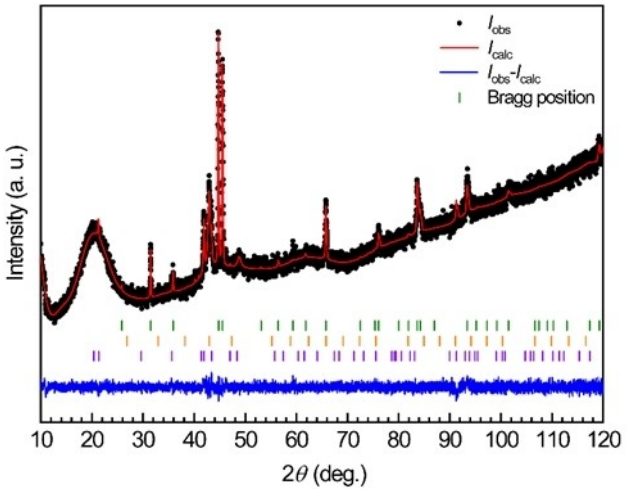

Figure 5. Powder X-ray diffraction pattern of the bulk pyrolysis product of **3**. Black dots represent the experimentally obtained data (I_{obs}), the red line shows the Rietveld fit (I_{calc}) while the blue line indicated the difference ($I_{calc}-I_{obs}$). The vertical bars show the Bragg positions of $Fe_{1.8}Ge$ (green), FeGe (orange, FeSi type) and FeGe (purple, CoSn type). The broad signal around $2\theta = 20°$ originates from the air sensitivity sample holder.

grains become larger (250 nm at 500 °C) and more irregular in shape with more pronounced edges, presumably caused by sintering and the formation of larger crystallites. At 650 °C, the surface morphology is dominated by irregularly shaped islands. Atomic force micrographs (Figure 6 H, I) show the formation of terraces. The film thickness of the samples was determined to 70–100 nm for an identical deposition times of 5 h. Elemental analysis by EDX shows a Fe–Ge ratio of 68:32 in case of a decomposition temperature of 350 °C, which is lower in Fe than the stoichiometric ratio in the precursor **4**. With rising target temperature, the iron content increases to 78:22 at 650 °C and hence approaches the molecular Fe–Ge ratio of compound **4**. These observations may imply the elimination of iron species as a side reaction at lower temperatures, while the cleavage of the CO ligands dominates at higher temperatures. Unfortunately, the carbon and oxygen percentages obtained from the EDX are unsuitably variable and can neither confirm nor exclude this possibility.

Phase analysis by powder XRD was performed for the films prepared at 350 °C (Figure S21) and 650 °C (Figure 7). In these cases, as well, there were no differences in powder diffraction patterns after exposure to air indicating air stability. Both powder patterns are characterized by a broad bump between 20° and 30° in 2θ, caused by the glass substrate and exhibit

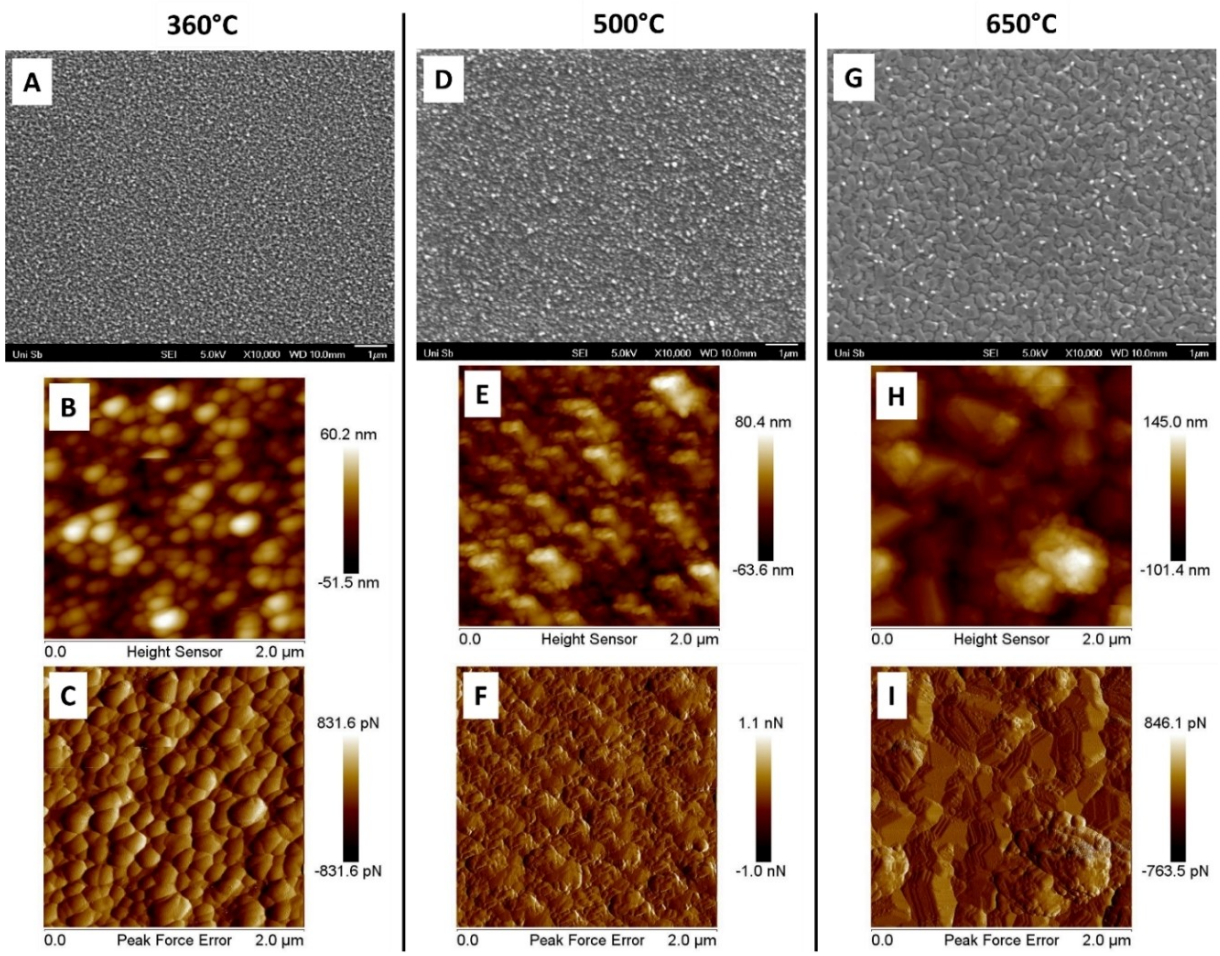

Figure 6. SEM and AFM images of Fe_xGe_{1-x} films by CVD with **4** as precursor at different target temperatures (**A**–**C** 360 °C, **D**–**F** 500 °C, **G**–**I** 650 °C).

Research Article
doi.org/10.1002/ejic.202300433

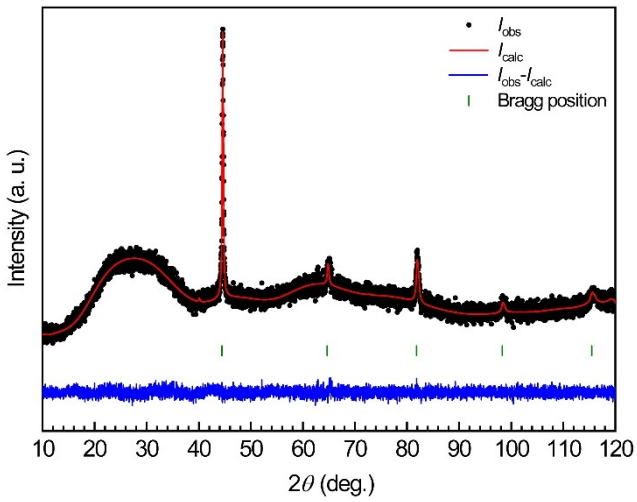

Figure 7. Powder X-ray diffraction pattern of the film obtained from precursor **4** and a target temperature of 650 °C. Black dots represent the experimentally obtained data (I_{obs}), the red line shows the Rietveld fit (I_{calc}) while the blue line indicated the difference ($I_{calc}-I_{obs}$). The vertical green bars show the Bragg positions. The broad signal around $2\theta = 20°$ originates from the glass substrate.

comparable powder patterns with the typical diffraction pattern of a cubic body centered structure (at 650 °C: $a = 288.07(6)$ pm; at 350 °C: $a = 288.13(6)$ pm). Upon refinement as *bcc*-Fe, differences in the intensities were observed that could be corrected using a Fe/Ge mixing on the sole crystallographic position. The refined composition was as Fe_xGe_{1-x} with $x = 0.61(3)$ for 350 °C and $x = 0.85(3)$ for 650 °C, which is in reasonable agreement with the EDX data. The observed lattice parameters are in line with other Fe/Ge solid solutions reported such as $Fe_{0.9}Ge_{0.1}$ with $a = 288.1$ pm[34] or $Fe_{0.91}Ge_{0.09}$ with $a = 288.15$ pm.[35]

Conclusions

In summary, we reported improved synthetic procedures for the germanium-iron carbonyl compounds $Ge[Fe_2(CO)_8]_2$ **4** and $[Fe_2(\mu\text{-}GeCl_2)_2(CO)_8]$ **2** including the first structural characterization of the latter. The dimer **2** is prone to dissociation in solution and therefore may be a useful synthon for the synthesis of base-adducts of the monomer. Proof-of-principle for this potentially general protocol was obtained by the preparation of $^{Me_2iPr_2}NHC \cdot GeCl_2 \cdot Fe(CO)_4$ **3**. Treatment of $GeCl_2 \cdot$1,4-dioxane complex with three equivalents of Fe_2CO_9 results in a mixture of compounds including the novel cluster compound $Cl_2Ge[Fe_2(CO)_8]Ge[Fe_2(CO)_8]$ **5**, which was isolated, albeit in low yields and fully characterized.

Most importantly, compounds **2**–**4** were tested as single-source precursors for binary iron germanium phases in chemical vapor deposition. While **2** and **4** indeed form dense films, precursor **3** requires high temperatures for sufficient evaporation and decomposition. Although the phase purity of the films is currently low, unambiguous XRD proof for the deposition of different iron/germanium species was obtained raising the prospects to apply CVD in this context through optimization of the deposition parameters and/or the use of related precursors.

Experimental Section

General: Unless otherwise stated, all syntheses and manipulations were carried out under an argon atmosphere by using a glove box or standard Schlenk techniques. Argon 5.0 gas was provided by Linde and used without further purification. The vacuum was generated by a slide vane rotary vacuum pump RZ 6 from Vakuubrand. All apparatus were evacuated until a pressure of 8×10^{-2} mbar or below was reached and filled with argon gas afterwards. This procedure was repeated three times. In case that objects had to be inserted into a glove box, the glove box's lock was evacuated for at least 3 min until it was filled with argon gas. Also, this procedure was repeated three times. Toluene, n-hexane and thf were purified by a PureSolve MD 5 solvent purification system by Inert Technology. Dry solvents were transferred with cannulas of stainless steel. $GeCl_2 \cdot$dioxane,[36] $^{Me_2iPr_2}NHC$[37] and **3**[16b] were prepared according to literature procedures.

Synthesis of di-μ-dichlorogermylene-bis(tetracarbonyliron) **2***:* $GeCl_2$/1,4-dioxane complex (1.1 g, 4.6 mmol) and $Fe_2(CO)_9$ (1.7 g, 4.6 mmol) were cooled to −78 °C and cold 100 mL thf were added. The greenish brown suspension was allowed to warm within 3 h and stirring continued overnight. All volatilities were removed *in vacuo*. The obtained solid was washed with 20 mL of n-hexane and then extracted with 40 mL of warm toluene. The red solution was stored at −20 °C for two days to obtain the product as orange crystals (1.7 g, 59 %). Single crystals suitable for X-ray diffraction were obtained from hot saturated hexane solution after keeping at room temperature for overnight as orange needles. $^{13}C\{^1H\}$ NMR (75.4 MHz, C_6D_6, 300 K): δ = 197.0, 204.0 ppm. IR (cyclohexane) ν = 2094, 2059, 2055, 2052, 602, 593 cm^{-1}. m.p.: 120 °C (dec.). Elemental analysis: Calcd. for $C_8Cl_4Fe_2Ge_2O_8$: C 15.43. Found: C 15.93; H 0.43.

Reaction of* 2 *with* $^{Me_2iPr_2}NHC$:*** 20 mg (0.032 mmol) of compound **2** were mixed in an NMR tube with 0.3 mL of C_6D_6 to obtain a yellow-orange suspension. A solution of 12 mg $^{Me_2iPr_2}NHC$ in 0.2 mL C_6D_6 was added, causing the precipitate to dissolve and a color-change to red. The ^1H- and $^{13}C\{^1H\}$ NMR data of the reaction mixture confirms the predominant formation of **3** alongside minor unidentified impurities by comparison with the published data.[16b]

Synthesis of Bis(diironoctacarbonyl)germanium **4***:* $GeCl_2$/1,4-dioxane complex (370 mg, 1.60 mmol) and $Fe_2(CO)_9$ (2.90 g, 8.02 mmol) were suspended in 50 mL of thf. The reaction mixture was stirred for three days. Afterwards, all volatile components were removed *in vacuo* and the residue was extracted with 40 mL of dichloromethane/hexane (1 : 1). The extract was reduced to half the volume and stored at −80 °C overnight, causing precipitation of the product as a red-to-orange powder in 58 % yield (688.8 mg). Single crystals suitable for X-ray analysis where obtained from a warm n-

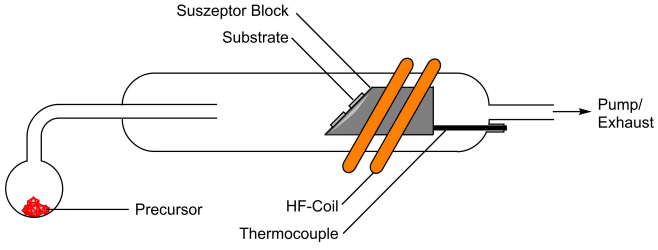

Figure 8. Schematic representation of the used CVD reactor.

Research Article
doi.org/10.1002/ejic.202300433

Table 2. Experimental conditions for chemical vapor depositions, with target temperature T_{target}, sublimation temperature T_{sub}, reactor pressure p and deposition time t.

Precursor	Substrate	T_{target} [°C]	T_{sub} [°C]	p [mbar]	t [h]
2	Si	650	90	$1 \cdot 10^{-2}$	2.5
2	glass	400	90	$7 \cdot 10^{-3}$	9
2	glass	650	90	$1 \cdot 10^{-2}$	20
3	Si	525	150	$7 \cdot 10^{-3}$	6
4	Si/glass	350	100	$2 \cdot 10^{-2}$	5
4	Si/glass	500	100	$2 \cdot 10^{-2}$	5
4	Si/glass	650	100	$2 \cdot 10^{-2}$	5

hexane solution. $^{13}C\{^1H\}$ NMR (75.4 MHz, C_6D_6, 300 K): $\delta =$ 208.6 ppm. IR (dichloromethane) $\nu = 2075, 2048, 2033, 2011\ cm^{-1}$. m.p. 180 °C (dec.). Elemental analysis: Calcd. for $C_{16}Fe_4GeO_{16}$: C 25.82. found 24.17, H 0.35.

Synthesis of μ-dichlorogermylene-μ-(diironoctacarbonyl)germylene-bis(tetracarbonyliron) **5***:* $GeCl_2$/1,4-dioxane complex (370 mg, 1.60 mmol) and $Fe_2(CO)_9$ (1.74 g, 4.81 mmol) were suspended in 30 mL of thf at −80 °C and stirred for 3 days, meanwhile the mixture was allowed to warm to room temperature. After removal of all volatile components *in vacuo*, the solid was purified by column chromatography (thoroughly dried silica, hexane). The separation should be performed as quickly as possible and can be done within 30 min. In order of elution, three fractions could be collected: first green fraction, $Fe_3(CO)_{12}$ (not isolated); second orange fraction, **4** (140 mg, 12%), third red fraction, **5** (47 mg, 7%). Single crystals suitable for XRD were grown from a warm n-hexane solution. $^{13}C\{^1H\}$ NMR (75.4 MHz, C_6D_6, 300 K): $\delta = 198.6, 200.8, 207.1$ ppm. IR (dichloromethane) $\nu = 2113, 2078, 2054, 2027, 2008\ cm^{-1}$. Elemental analysis: Calcd. for $C_{16}Cl_2Fe_4Ge_2O_{16}$: C, 21.65. Found: C, 23.18; H 0.29.

Bulk pyrolysis of **2***:* In a glovebox, 600 mg of compound **2** were ground and heated to 650 °C within 10 h in a tube furnace (FRH-70/250/1100 by Linn High Therm) with a constant flow of argon (*ca.* 100 L h^{-1}). After 12 h, the gas flow was stopped and the sample tempered at 650 °C for additional 7 days. Pyrolysis was carried out in unglazed porcelain combustion boats supplied by VWR.

Bulk pyrolysis of **3** was performed analogously, while the pyrolysis temperature of 500 °C was reached after 10 h and held for 12 h under constant argon flow. The sample was subsequently tempered at 500 °C for 6 days without an applied argon flow.

Deposition procedure. Chemical vapor deposition was performed in a home-built horizontal cold-wall CVD reactor (Figure 8). The used substrates were placed on a susceptor block made of graphite and heated inductively by a HTG1500/0,5 high frequency generator by Linn High Therm. All glass apparatus are made of borosilicate glass. The complete setup is arranged in a thermically isolated box and can be heated *via* a heating installation. An RZ 6 rotary vane pump from Vacuubrand was used to apply an interior pressure of at 10^{-2} mbar or lower. Detailed experimental parameters are given in Table 2.

Glass substrates cut microscopy slides by Carl Roth were used for p-XRD measurements. The slides were rinsed with demineralized water and acetone and stored in an oven at 120 °C before use. Samples with silicon substrates were used for SEM/EDX. Silicon wafers (cut in 10×10 mm chips, <111> p-type, Ted Palla, Inc.) were used without further cleaning.

Supporting Information

Experimental details, plots of NMR spectra, plots of IR spectra, thermogravimetric analysis, additional plots of powder-XRD, plots of EDX spectra, and crystallographic data.

The authors have cited additional references within the Supporting Information.[36–39]

Deposition Number(s) 2207556 (for **2**) and 2207554 (for **5**) contain the supplementary crystallographic data for this paper. These data are provided free of charge by the joint Cambridge Crystallographic Data Centre and Fachinformationszentrum Karlsruhe Access Structures service.

Acknowledgements

We thank the Alexander von Humboldt-Foundation for a Research Group Linkage Grant. Instrumentation and technical assistance for this work were provided by the Service Center X-ray Diffraction, with financial support from Saarland University and German Science Foundation (project number INST 256/506-1 and INST 256/349-1). We thank Mana A. Mohamed for TGA-IR measurements and Dr. Jörg Schmauch for SEM imaging and EDX. Open Access funding enabled and organized by Projekt DEAL.

Conflict of Interests

The authors declare no conflict of interest.

Data Availability Statement

The data that support the findings of this study are available in the supplementary material of this article.

Keywords: Chemical vapor deposition · germanium · Iron · Thin layers · Transition metal tetrelides

[1] P. J. Schurer, N. J. G. Hall, A. H. Morrish, *Phys. Rev. B* **1978**, *18*, 4860–4874.

[2] a) J. Tang, C.-Y. Wang, M.-H. Hung, X. Jiang, L. T. Chang, L. He, P.-H. Liu, H.-J. Yang, H. Y. Tuan, L.-J. Chen, K. L. Wang, *ACS Nano* **2012**, *6*, 5710–5717; b) M. E. Schlesinger, *Chem. Rev.* **1990**, *90*, 607–628.
[3] N. A. Porter, J. C. Gartside, C. H. Marrows, *Phys. Rev. B* **2014**, *90*, 024403.
[4] X. Z. Yu, N. Kanazawa, Y. Onose, K. Kimoto, W. Z. Zhang, S. Ishiwata, Y. Matsui, Y. Tokura, *Nat. Mater.* **2011**, *10*, 106–109.
[5] K. Kanematsu, T. Ohoyama, *J. Phys. Soc. Jpn.* **1965**, *20*, 236–242.
[6] a) G. Lungu, N. Apostol, L. Stoflea, R. Costescu, D. Popescu, C. Teodorescu, *Materials* **2013**, *6*, 612–625; b) J. L. Lensch-Falk, E. R. Hemesath, F. J. Lopez, L. J. Lauhon, *J. Am. Chem. Soc.* **2007**, *129*, 10670–10671.
[7] D. D. Vaughn, D. Sun, J. A. Moyer, A. J. Biacchi, R. Misra, P. Schiffer, R. E. Schaak, *Chem. Mater.* **2013**, *25*, 4396–4401.
[8] a) A. Sodreau, S. Mallet-Ladeira, S. Lachaize, K. Miqueu, J.-M. Sotiropoulos, D. Madec, C. Nayral, F. Delpech, *Dalton Trans.* **2018**, *47*, 15114–15120; b) A. Sodreau, N. Lentz, M. Frutos, S. Mallet-Ladeira, C. Nayral, F. Delpech, D. Madec, *Chem. Commun.* **2019**, *55*, 9539–9542.
[9] S. Wolf, A. Egeberg, J. Treptow, C. Feldmann, *ChemistryOpen* **2021**,*10*, 171–180.
[10] a) H. Yoon, A. T. Lee, E.-A. Choi, K. Seo, N. Bagkar, J. Cho, Y. Jo, K. J. Chang, B. Kim, *J. Am. Chem. Soc.* **2010**, *132*, 17447–17451; b) M. J. Stolt, Z.-A. Li, B. Phillips, D. Song, N. Mathur, R. E. Dunin-Borkowski, S. Jin, *Nano Lett.* **2016**, *17*, 508–514.
[11] a) A. N. Gleizes, *Chem. Vap. Deposition* **2000**, *6*, 155–173; b) A. L. Schmitt, J. M. Higgins, J. R. Szczech, S. Jin, *J. Mater. Chem.* **2010**, *20*, 223–235.
[12] a) W. Petz, *Chem. Rev.* **1986**, *86*, 1019–1047; b) J. Baumgartner, C. Marschner, *Rev. Inorg. Chem.* **2014**, *34*, 119–152.
[13] R. Kummer, W. A. G. Graham, *Inorg. Chem.* **1968**, *7*, 1208–1214.
[14] T. J. Marks, A. R. Newman, *J. Am. Chem. Soc.* **1973**, *95*, 769–773.
[15] P. Jutzi, W. Steiner, *Chem. Ber.* **1976**, *109*, 3473–3479.
[16] a) M. El Ezzi, T.-G. Kocsor, F. D'Accriscio, D. Madec, S. Mallet-Ladeira, A. Castel, *Organometallics* **2015**, *34*, 571–576; b) A. Jana, V. Huch, H. S. Rzepa, D. Scheschkewitz, *Organometallics* **2014**, *34*, 2130–2133.
[17] A. Maiti, D. Mandal, I. Omlor, D. Dhara, L. Klemmer, V. Huch, M. Zimmer, D. Scheschkewitz, A. Jana, *Inorg. Chem.* **2019**, *58*, 4071–4075.
[18] D. Mandal, D. Dhara, A. Maiti, L. Klemmer, V. Huch, M. Zimmer, H. S. Rzepa, D. Scheschkewitz, A. Jana, *Chem. Eur. J.* **2018**, *24*, 2873–2878.
[19] S. G. Anema, K. M. Mackay, B. K. Nicholson, M. Van Tiel, *Organometallics* **1990**, *9*, 2436–2442.
[20] A. Bonny, K. M. MacKay, *J. Chem. Soc. Dalton Trans.* **1978**, 506–511.
[21] S. G. Anema, K. M. Mackay, B. K. Nicholson, *Inorg. Chem.* **1989**, *28*, 3158–3164.
[22] R. S. Simons, K. J. Galat, J. D. Bradshaw, W. J. Youngs, C. A. Tessier, G. Aullón, S. Alvarez, *J. Organomet. Chem.* **2001**, *628*, 241–254.
[23] D. Melzer, E. Weiss, *J. Organomet. Chem.* **1983**, *255*, 335–344.
[24] A. S. Batsanov, L. V. Rybin, M. I. Rybinskaya, Yu. . Struchkov, I. M. Salimgareeva, N. G. Bogatova, *J. Organomet. Chem.* **1983**, *249*, 319–326.
[25] S. G. Anema, G. C. Barris, K. M. Mackay, B. K. Nicholson, *J. Organomet. Chem.* **1988**, *350*, 207–215.
[26] C. Vollmer, C. Janiak, *Coord. Chem. Rev.* **2011**, *255*, 2039–2057.
[27] K. Lubitz, V. Sharma, S. Shukla, J. H. J. Berthel, H. Schneider, C. Hoßbach, U. Radius, *Organometallics* **2018**, *37*, 1181–1191.
[28] J. Sinclair, G. Dai, R. McDonald, M. J. Ferguson, A. Brown, E. Rivard, *Inorg. Chem.* **2020**, *59*, 10996–11008.
[29] H. O. Pierson, *Handbook of Chemical Vapor Deposition (CVD)*, Noyes Park Ridge, NJ **1992**.
[30] Z. V. Dobrokhotova, P. S. Koroteev, A. V. Saushev, G. G. Aleksandrov, V. M. Novotortsev, S. E. Nefedov, M. P. Egorov, *Russ. Chem. Bull.* **2003**, *52*, 1681–1687.
[31] M. Veith, S. Kneip, *J. Mater. Sci. Lett.* **1994**, *13*, 335–337.
[32] P. Villars, K. Cenzual, *Pearson's crystal data-crystal structure database for inorganic compounds* ASM International, Materials Park, Ohio (USA), **2021**.
[33] Based on the presented TGA data, a target temperature of 220 °C is sufficient. Nevertheless, a target temperature of 360 °C was used for sake of reproducibility, since lower temperatures suffer from instabilities in the used induction furnace.
[34] E. P. Yelsukov, G. N. Konygin, O. M. Nemtsova, V. E. Porsev, *J. Magn. Magn. Mater.* **2007**, *308*, 171–176
[35] M. Huang, T. A. Lograsso, *Appl. Phys. Lett.* **2009**, *95*, 171907.
[36] C. A. Roskamp, E. J. Roskamp, *Encyclopedia of Reagents for Organic Synthesis*, John Wiley & Sons, Ltd, Chichester, UK, **2001**.
[37] N. Kuhn, T. Kratz, *Synthesis* **1993**, *6*, 561–562.
[38] *Topas 5*; Bruker AXS: Karlsruhe (Germany) **2014**.
[39] a) G. M. Sheldrick, *Acta Crystallogr. Sect. A* **2007**, *64*, 112–122; b) G. M. Sheldrick, *Acta Crystallogr. Sect. C* **2015**, *71*, 3–8; c) C. B. Hübschle, G. M. Sheldrick, B. Dittrich, *J. Appl. Crystallogr.* **2011**, *44*, 1281–1284.

Manuscript received: July 17, 2023
Revised manuscript received: July 27, 2023
Accepted manuscript online: July 31, 2023
Version of record online: August 25, 2023